

# Nanoconfinement-Induced Giant Electrocaloric Effect in Ferroelectric Polymer Nanowire Array Integrated with Aluminum Oxide Membrane to Exhibit Record Cooling Power Density

Guangzu Zhang, Lingxi Weng, Zhaoyao Hu, Yang Liu, Runxi Bao, Peng Zhao, Hao Feng, Nuo Yang, Ming-Yu Li, Sulin Zhang, Shenglin Jiang,\* and Qing Wang\*

The electrocaloric effect (ECE) offers a unique mechanism to realize environmentally friendly and highly efficient solid-state cooling that completely differs from the conventional vapor-compression refrigeration. Here a new class of hybrid films composed of ferroelectric polymer nanowire array and anodic aluminum oxide (AAO) membrane is reported, which displays pronounced ECE driven by relatively low electric fields. Under confinement and orientation of AAO channels on the crystallization of the polymer, the polymer nanowire array shows substantially enhanced ECE that is about three times that of the corresponding thin films. Simultaneously, the integrated AAO membrane forms thermally conducting channels for the polymer nanowires, enabling the efficient transfer of cooling energy and operation of the EC materials under high frequencies, which are unattainable based on the currently available EC structures. Consequently, the integrated polymer nanowire–AAO hybrid film exhibits the state-of-the-art cooling power density, outperforming the current ferroelectric polymers, ceramics, and composites. This work opens a new route for the development of scalable, high-performance EC materials for next-generation refrigeration.


Refrigeration is indispensable in modern society, such as air-conditioning in buildings, fridges for food storage, and thermal management of electronics.<sup>[1]</sup> The current cooling technology is still mainly based on the mechanical vapor-compression invented more than one century ago despite its high energy consumption, poor cooling efficiency, and negative environmental effects.<sup>[2,3]</sup> Nowadays, cooling contributes more than 6%

to the global electric energy consumption and concurrently emits ≈600 000 tons of ozone-depletion and greenhouse gases into the atmosphere every year.<sup>[4,5]</sup> The caloric effects, i.e., the reversible thermal changes induced by phase transition in ferroic materials, including magnetocaloric effect (MCE), electrocaloric effect (ECE), and mechanocaloric effect (mCE), offer promising alternatives for the next-generation ecofriendly refrigeration with high cooling efficiencies.<sup>[6–15]</sup>

Pronounced ECE has been obtained in both inorganic ferroelectric materials including bulk ceramics and single crystals and ferroelectric polymers such as poly(vinylidene fluoride-co-trifluoroethylene) P(VDF-TrFE) and poly(vinylidene fluoride-ter-trifluoroethylene-ter-chloro-fluoroethylene) (PVDF-TrFE-CFE) over the last decades.<sup>[16–21]</sup> In particular, ferroelectric polymers hold significant potential for practical cooling applications owing to their intrinsic processability, scalability, and lightweight advantages. Moreover, compared to inorganic counterparts, ferroelectric polymers enjoy larger changes of isothermal entropy ( $\Delta S$ ) and higher cooling energy density ( $Q$ ,  $Q = T\Delta S$ , where  $T$  is the environment temperature).<sup>[22,23]</sup> For example, with an adiabatic temperature change ( $\Delta T$ ) of 1 K,  $\Delta S$  of P(VDF-TrFE) and P(VDF-TrFE-CFE) is  $\approx 10 \text{ kJ K}^{-1} \text{ m}^{-3}$ , which is two times that of

Prof. G. Zhang, L. Weng, Z. Hu, R. Bao, Dr. M.-Y. Li, Prof. S. Jiang  
School of Optical and Electronic Information  
Huazhong University of Science and Technology  
Wuhan, Hubei 430074, China  
E-mail: jsl@hust.edu.cn

Prof. G. Zhang, Dr. M.-Y. Li  
Engineering Research Center for Functional Ceramics  
Ministry of Education  
Huazhong University of Science and Technology  
Wuhan 430074, China

 The ORCID identification number(s) for the author(s) of this article can be found under <https://doi.org/10.1002/adma.201806642>.

Dr. Y. Liu, Prof. Q. Wang  
Department of Materials Science and Engineering  
The Pennsylvania State University  
University Park, PA 16802, USA  
E-mail: wang@matse.psu.edu

P. Zhao, Prof. S. Zhang  
Department of Engineering Science and Mechanics  
The Pennsylvania State University  
University Park, PA 16802, USA

H. Feng, Prof. N. Yang  
School of Energy and Power Engineering  
Huazhong University of Science and Technology  
Wuhan, Hubei 430074, China

DOI: 10.1002/adma.201806642

the lead zirconate titanate (PZT) ceramic film.<sup>[6,9,22]</sup> Note that  $Q$  and  $\Delta S$  are of prime importance for refrigeration since they directly determine the heat absorbed by a unit EC material in each operating cycle.<sup>[15,24]</sup>

On the other hand, the EC strength represented by  $|Q/\Delta E|$ ,  $|\Delta S/\Delta E|$ , and  $|\Delta T/\Delta E|$ , where  $E$  is the applied electric field, of ferroelectric polymers is inferior to those of the inorganic ferroelectrics,<sup>[18,25]</sup> indicating that the ECE in polymers can only be driven by high electric fields.<sup>[6,22]</sup> The required high operation field in ferroelectric polymers not only complicates operation but also risks the stability and lifetime of the EC devices. In addition, polymers are well-known thermal insulators with thermal conductivities of 0.1–0.4 W m<sup>-1</sup> K<sup>-1</sup>, which are about only one-tenth those of the inorganic ferroelectric materials.<sup>[26]</sup> The thermal conductivity of the EC materials is being recognized to play a critical role in the cooling performance since it determines the heat flow in the materials and the heat exchange between the materials and external loads. For the materials with poor thermal conductivities, the energy yielded from ECE might be partially or even fully offset by the heat generated in the entropy-decrement process (Note S1, Supporting Information), resulting in much reduced cooling energy and efficiency.<sup>[27,28]</sup> More recently, the polymer composite approach has been developed to address the intrinsic drawbacks of the ferroelectric polymers for EC cooling.<sup>[29–31]</sup>

In this work, we report a hybrid film composed of P(VDF-TrFE-CFE) nanowire array and anodic aluminum oxide (AAO) membranes, which exhibits a superior EC cooling power density when compared to the current ferroelectric ceramics, polymers, and ceramic–polymer composites. The confinement on the ferroelectric polymer chains created by AAO leads to a two-fold improvement in the EC strength of the nanowire array relative to that of the conventional polymer films. Concomitantly, the high-temperature-annealed AAO membrane with a high thermal conductivity ingeniously functions as highly desirable heat-transfer channels for the embedded polymer nanowires, allowing the EC cooling energy to be absorbed efficiently by the heat load with a neglectable loss. This strategy is scalable and has simultaneously addressed several long-standing challenges, including operation field and thermal transfer, in the polymer-based EC cooling devices.<sup>[9,28]</sup>

The P(VDF-TrFE-CFE) nanowire arrays were fabricated by a solution-wetting approach with the AAO nanoporous membrane, as schematically illustrated in **Figure 1a**. High-quality AAO membranes consisting of vertical nanochannels with a mean diameter of 100 nm and a length of 100  $\mu$ m were obtained (Figure 1b–e) via a two-step anodization electrochemical reaction and annealing process.<sup>[32]</sup> The porosity of the AAO membrane is estimated to be  $\approx 55\%$ . By dripping P(VDF-TrFE-CFE)/dimethylformamide (DMF) solution into the nanochannels of the AAO membrane, a uniform P(VDF-TrFE-CFE) array with parallelly aligned nanowires was produced, as corroborated in Figure 1f–i. The breakdown strength of the nanowire array is around 60 MV m<sup>-1</sup>. For the comparison purpose, a conventional P(VDF-TrFE-CFE) thin film with a thickness of 100  $\mu$ m was prepared through the solution-casting method (see Experimental Section for details).

**Figure 2** summarizes the EC characteristics of the P(VDF-TrFE-CFE) nanowire array and thin film measured at room

temperature, including  $Q$ ,  $\Delta T$  and  $\Delta S$ , and the EC strength. Apparently, considerably enhanced ECE has been observed in the P(VDF-TrFE-CFE) nanowires at relatively low electric fields. For example, under an electric field of 30 MV m<sup>-1</sup>, the nanowire array shows a  $Q$  of 1.8 MJ m<sup>-3</sup>, a  $\Delta T$  of 0.7 °C and a  $\Delta S$  of 6.0 kJ m<sup>-3</sup> K<sup>-1</sup>, all of which are approximately three times those of the P(VDF-TrFE-CFE) thin film (Figure 2a). More interestingly, the EC strength of the nanowires exceeds that of the polymer film (Figure 2b), e.g., a  $|Q/\Delta E|$  of 132 kJ MV<sup>-1</sup> m<sup>-2</sup> versus 45 kJ MV<sup>-1</sup> m<sup>-2</sup> of the film at 50 MV m<sup>-1</sup>, and reaches the same level of some inorganic ferroelectrics and recently developed ceramic–polymer composites (**Table 1**). The enhanced EC strength significantly lowers the threshold electric field required to achieve sizable EC responses. For example, as presented in Figure 2b, a  $\Delta T$  of  $\approx 2.5$  °C can be obtained in the nanowire array with an applied field of 50 MV m<sup>-1</sup>, whereas only a  $\Delta T$  of 0.8 °C is found in the P(VDF-TrFE-CFE) film under the same field.

The notable improvement of the ECE of the ferroelectric polymer nanowires has been attributed to the unique crystallization behavior arising from the confinement of the AAO nanochannels.<sup>[40]</sup> While the P(VDF-TrFE-CFE) nanowires possess the same ferroelectric phase structure to the film, as identified by X-ray diffraction (XRD) (**Figure 3a**), they exhibit different crystallinity, melting temperature, and average crystal size (Figure S2 and Table S1, Supporting Information). The confinement effect leads to an apparent reduction in the crystal size from 31.8 nm of the film to 19.7 nm of the nanowires calculated from the (200)/(100) XRD characteristic peak with the Scherrer's equation (Table S1, Supporting Information).<sup>[41]</sup> The melting temperature of the nanowire measured by differential scanning calorimetry (DSC) is about 3 °C lower than that of the film (i.e., 128 °C), further indicating a smaller crystal size of the nanowire array (Figure S2, Supporting Information).<sup>[42]</sup> The enthalpy of fusion calculated from the integration of the DSC melting endothermic peak in the nanowire array is  $\approx 1.2$  times that of the film, signifying a higher crystallinity induced by the confinement (Figure S2, Supporting Information).<sup>[43]</sup> Both increased crystallinity and decreased crystal size are conducive to improve the electrical polarization in ferroelectric polymers because enhanced crystallinity offers higher polarizability and the dipoles in smaller crystals are easier to be aligned by the applied electric fields.<sup>[44,45]</sup> Indeed, as shown in the polarization–electric field ( $P$ – $E$ ) loops (Figure S3a, Supporting Information), the polarization of the ferroelectric polymer in the form of nanowire array is much higher than that in the film, e.g., 5.4 versus 2.8  $\mu$ C cm<sup>-2</sup> measured at 60 MV m<sup>-1</sup>, which decreases more sharply with the increase of temperature than that of the film (Figure S3b, Supporting Information). Since ECE originates from the entropy change of dipoles induced by electric fields,<sup>[5,6]</sup> the higher polarization, steeper polarization–temperature curve and smaller crystallites of the nanowires lead to the improved ECE,<sup>[46–49]</sup> especially at relatively low electric fields (Notes S2 and S3, Supporting Information).

Additionally, it is found that the nanochannel-driven alignment of the molecular chains and orientation of the crystallites of ferroelectric polymers plays a key role in the ECE of the nanowire array. As illustrated in the 2D XRD patterns (Figure 3c), the nanowire gives the diffraction arcs on both equators,

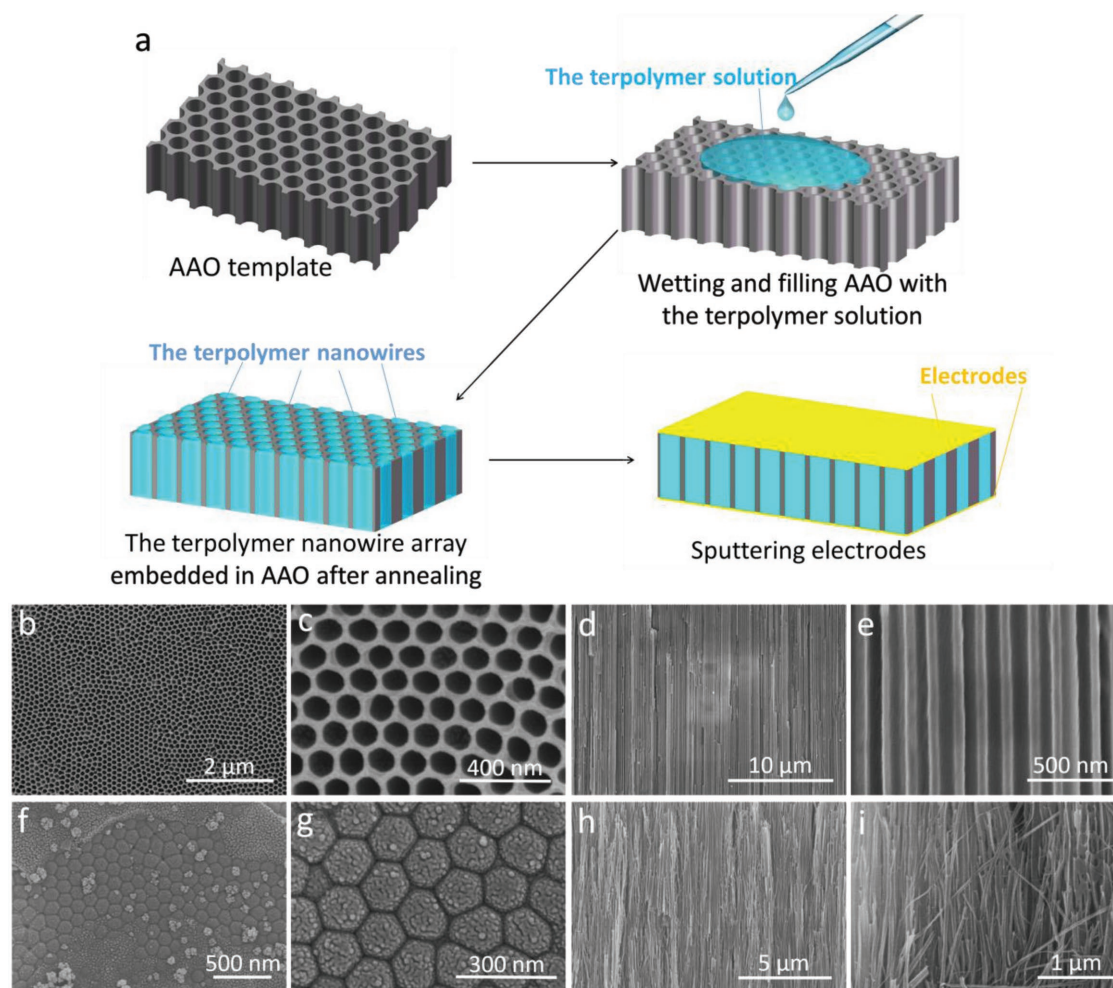


**Figure 1.** a) Schematic illustration of the preparation of the polymer nanowire array. b) Top-view SEM image of the AAO membrane. c) The magnified image of the AAO surface. d) The cross-sectional SEM of the AAO membrane. e) The magnified image of the cross-sectional view of the AAO channels. f) The surface of the AAO membrane filled with P(VDF-TrFE-CFE) terpolymer. g) The magnified top-view SEM of the polymer nanowires in the AAO template. h) The SEM of the polymer nanowires embedded in the AAO nanochannels. i) The polymer nanowires after removing the AAO template.

suggestive of the molecular chain direction of the crystals being aligned within the nanochannels. Comparatively, the polymer film displays a continuous diffraction ring (Figure 3b), indicative of its random orientation of crystallites. As substantiated by the molecular thermodynamic simulations,<sup>[50–53]</sup> the walls of the nanochannels give a strong spatial restriction to the polymer nanowires and “freeze” their axial surface layer. Since the conformational entropy of the crystal whose molecular chains extend along the transverse section of the nanochannels is much lower than the entropy of those chains aligned parallel to the trenches under the channel-wall restriction, the nanoconfinement compels the inner molecular chains of the nanowires to crystallize within the  $a$ – $c$  plane, leading to a preferential crystallographic orientation in which the lamellas stack parallel to the nanochannels.<sup>[54–57]</sup> As illustrated in Figure 3d, the  $b$  axis, the polar axis of the ferroelectric polymer, is orientated along the direction of the nanochannels and parallel to the applied electric field (Figure 3d). Consequently, the dipoles on the aligned molecular chains are readily to be rotated around the chains ( $c$ -axis) by the applied fields. The strong coupling of

the dipoles and applied electric field in the nanowires thus significantly lowers the threshold electric field required for large polarization;<sup>[55,56]</sup> this rationalizes the improved EC strength found in the nanowires.

In addition to the marked room-temperature EC responses, practical cooling devices necessitate the ferroelectric materials to maintain strong ECE over a wide temperature range. Generally, for the EC cooling devices run in the Ericsson cycle mode, high cooling efficiency (i.e., the ratio of the cooling energy generated through the ECE to the electrical work consumed by the EC material) can only be attained with a stable  $|\Delta S|$  when the EC material operating between the hot and cold sides of a refrigerator (Figure S4, Supporting Information).<sup>[58]</sup> Besides, for a material whose ECE is only valid in a narrow temperature range, an intricate cascaded configuration has to be designed to obtain a decent temperature span, in which each EC element operates around its most effective temperature (Figure S5, Supporting Information).<sup>[59]</sup> As plotted in Figure S6 (Supporting Information), the ECE of the P(VDF-TrFE-CFE) film is maintained in the temperature ranging from 0 °C to 60 °C with a



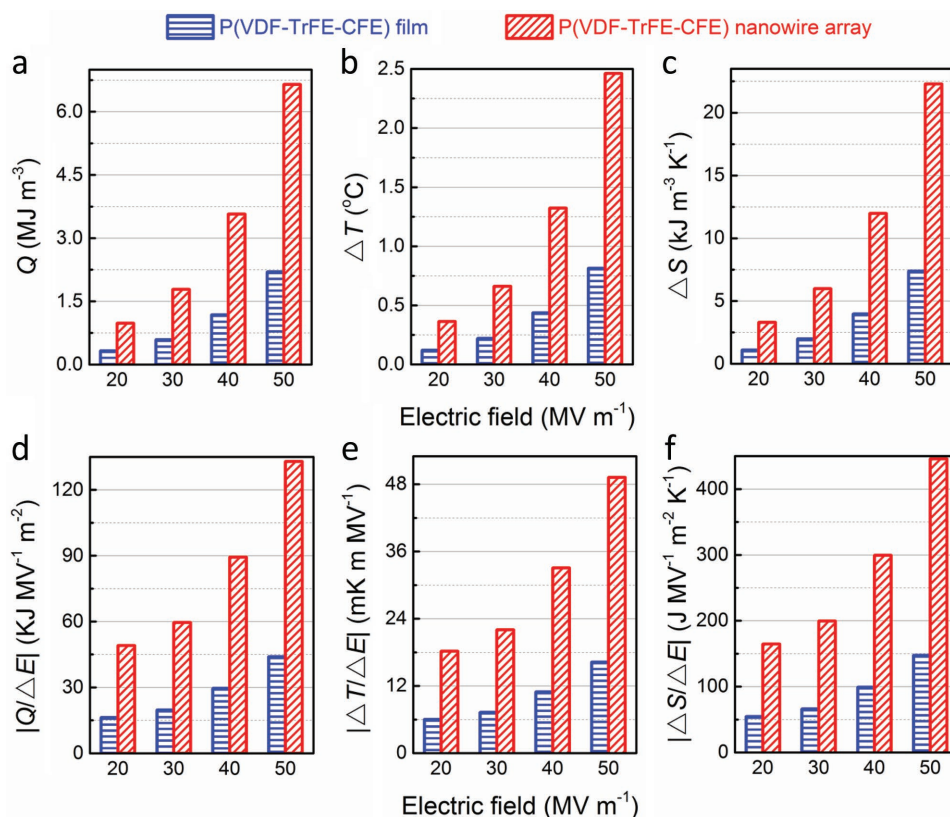


**Figure 2.** a)  $Q$ , b)  $\Delta T$ , c)  $\Delta S$ , d)  $|Q|/\Delta E$ , e)  $|\Delta T|/\Delta E$ , and f)  $|\Delta S|/\Delta E$  of the P(VDF-TrFE-CFE) nanowire array and film under different electric fields measured at room temperature.

stability of  $\approx 80\%$ , owing to its relaxor ferroelectric nature.<sup>[29]</sup> Surprisingly, it is found that the nanoconfinement effect yields further improvement in the temperature stability of the ECE of the nanowire array to  $\approx 95\%$  (Figure S6c, Supporting Information). As characterized by the Fourier transform infrared spectroscopy (FTIR, Figure S7a, Supporting Information), the content of the  $T_m$  ( $m > 4$ ,  $T$ : *trans*) conformation at  $\approx 1288\text{ cm}^{-1}$  corresponding to normal ferroelectrics decreases considerably from 16% of the film to 2% of the nanowire while the content of the TG ( $G$ : *gauche*) at  $\approx 618\text{ cm}^{-1}$  related to the relaxor phase increases from 49% of the film to 58% of the nanowire (Figure S7b, Supporting Information), thus confirming the added relaxor characteristics in the nanowire. A broad dielectric constant peak presented in the dielectric spectra of the film and the nanowire array moves toward high temperatures with increasing frequency (Figure S8a,b, Supporting Information), indicative of their relaxor nature. To further compare the relaxor behavior of the nanowire array and film, the degree of diffusion constant ( $\gamma$ ) was acquired according to the Curie–Weiss relationship.<sup>[60,61]</sup> As shown in Figure S8c,d (Supporting Information),  $\gamma$  of the nanowire array, i.e., 1.71, is higher than that of the film, i.e., 1.60, suggesting its stronger relaxor characteristics. Furthermore, the relaxor activation energy ( $E_a$ ) was calculated from the dielectric spectra using the Arrhenius plots of  $\log(\text{peak frequency})$  versus the  $1/\text{peak temperature}$ .<sup>[62]</sup> As shown in Figure S8c (Supporting Information),  $E_a$  of the nanowire array is  $\approx 5.34\text{ eV}$ , which is lower than that of the

polymer film (i.e.,  $\approx 6.77\text{ eV}$ ), again demonstrating the facile orientation of dipoles under the field and the strengthened relaxor behavior of the nanowires.

To further confirm the practicability of the polymer nanowire array, the aging test has been carried out. As shown in Figure S9 (Supporting Information), discernible degradation in the  $Q$ ,  $\Delta T$ , and  $\Delta S$  has not been observed in the array after 10 000 continuous operating cycles when subjected to an electric field of  $50\text{ MV m}^{-1}$ .

The ECE of the nanowire array has been investigated by changing the diameter of the nanowire. As presented in Figures S10–S14 (Supporting Information), the AAO membranes with different pore sizes varying from 30 to 400 nm were fabricated in the anodization electrochemical process. Inferior ECE is observed in the nanowire array prepared from the channels with diameters  $< 100\text{ nm}$  due to incomplete filling of the polymer melt in the channels (Figures S13 and S14, Supporting Information). It is found that the ECE of the nanowire array decreases with the increase of the nanowire diameter from 100 to 400 nm, owing to weakening the confinement of the polymer chain and reducing polarization with the increased pore size of the AAO membranes. The ECE of the 400 nm diameter nanowire array is very close to that of the thin film as shown in Figure S15 (Supporting Information).

Besides the nanoconfinement effect, the AAO channels simultaneously create efficient heat conduction pathways for the polymer nanowire array. As shown in Figure S16

**Table 1.** The ECE of ferroelectric materials at room temperature.

Materials	$Q^a$	$\Delta T^b$	$\Delta S^c$	$\Delta E^d$	$ Q/\Delta E ^e$	$ \Delta T/\Delta E ^f$	$ \Delta S/\Delta E ^g$	Method	Refs.
0.9 PMN-0.1 PT thin film	3.0	1.2	9.9	50.8	58.8	24.1	195	Maxwell relation	[33]
BNKT thin film	52	17	171	112	464	151	1527	Maxwell relation	[34]
BZT thin film	182	45	492	101	1800	445	4871	Maxwell relation	[35]
BaTiO <sub>3</sub> MLCC	2.2	0.5	5.7	30	73.3	16.7	190	Thermometer	[36]
PLZT(8/65/35) bulk ceramic	0.39	0.16	1.3	3	130.0	53.3	433	Maxwell relation	[37]
0.45BZT–0.55BCT single crystal	0.08	0.04	0.27	1.2	66.7	33.3	225	Maxwell relation	[18]
P(VDF-TrFE) film	2.4	0.7	7.2	50	48.0	14.0	144	Heat flux sensor	[38]
P(VDF-TrFE-CFE) film	2.4	1.0	8.1	50	48.0	20.0	162	Heat flux sensor	[38]
P(VDF-TrFE)/P(VDF-TrFE-CFE) blend film	8.0	3.0	27.0	50	160.0	60.0	540	Heat flux sensor	[21]
P(VDF-TrFE-CFE)/BST composite film	8.7	3.0	28.0	50	174.0	60.0	560	Heat flux sensor	[29]
P(VDF-TrFE-CFE)/PMN-PT composite film	6.0	2.0	20.0	50	120.0	40.0	400	Heat flux sensor	[39]
Polymer nanowire array	6.6	2.5	22.1	50	132.0	50.0	442	Heat flux sensor	This work

The units of  $Q$ ,  $\Delta T$ ,  $\Delta S$ ,  $\Delta E$ ,  $|Q/\Delta E|$ ,  $|\Delta T/\Delta E|$ , and  $|\Delta S/\Delta E|$  are <sup>a)</sup>MJ m<sup>-3</sup>, <sup>b)</sup>°C, <sup>c)</sup>kJ m<sup>-3</sup> K<sup>-1</sup>, <sup>d)</sup>MV m<sup>-1</sup>, <sup>e)</sup>kJ MV<sup>-1</sup> m<sup>-2</sup>, <sup>f)</sup>mK m MV<sup>-1</sup>, and <sup>g)</sup>MV<sup>-1</sup> m<sup>-2</sup> K<sup>-1</sup>, respectively.

(Supporting Information), a thermal conductivity of 6 W m<sup>-1</sup> K<sup>-1</sup> was found in the high-temperature annealed AAO membrane, which is more than 30 times that of the ferroelectric polymer and around four folders higher than that of the ferroelectric ceramics.<sup>[63,64]</sup> Finite element simulations were

conducted to quantitatively analyze the heat transfer processes in the pristine polymer and the integrated nanowire array–AAO hybrid films. Different from the conventional EC structures in which the cooling energy is transferred entirely through the film (Figure 4a–VI–VIII), the cooling energy generated in the

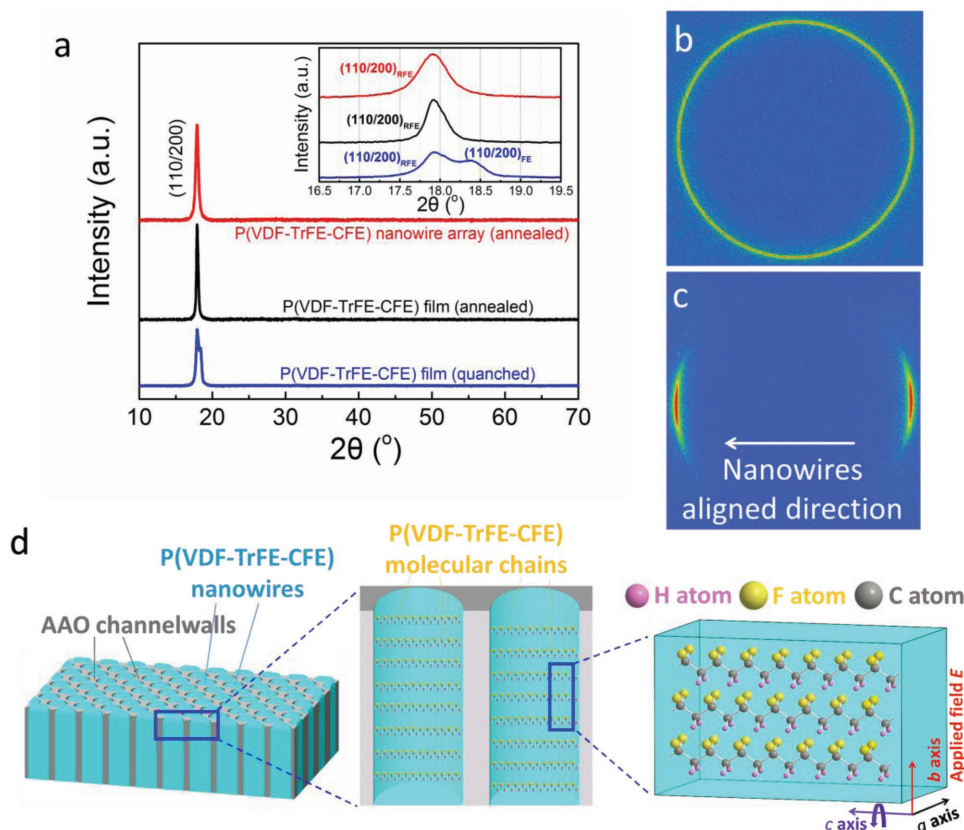


**Figure 3.** a) XRD patterns of the P(VDF-TrFE-CFE) nanowire array and films. The nanowire array and film present single sharp peak corresponding to the relaxor phase (RFE) upon annealing, while the quenched film shows a split peak related to the relaxor and normal ferroelectric phases (RFE and FE). b, c) 2-D XRD spectra of the P(VDF-TrFE-CFE) terpolymer film and nanowire array. d) Schematic illustration of the molecular chain orientation in the nanowires compelled by the AAO confinement.

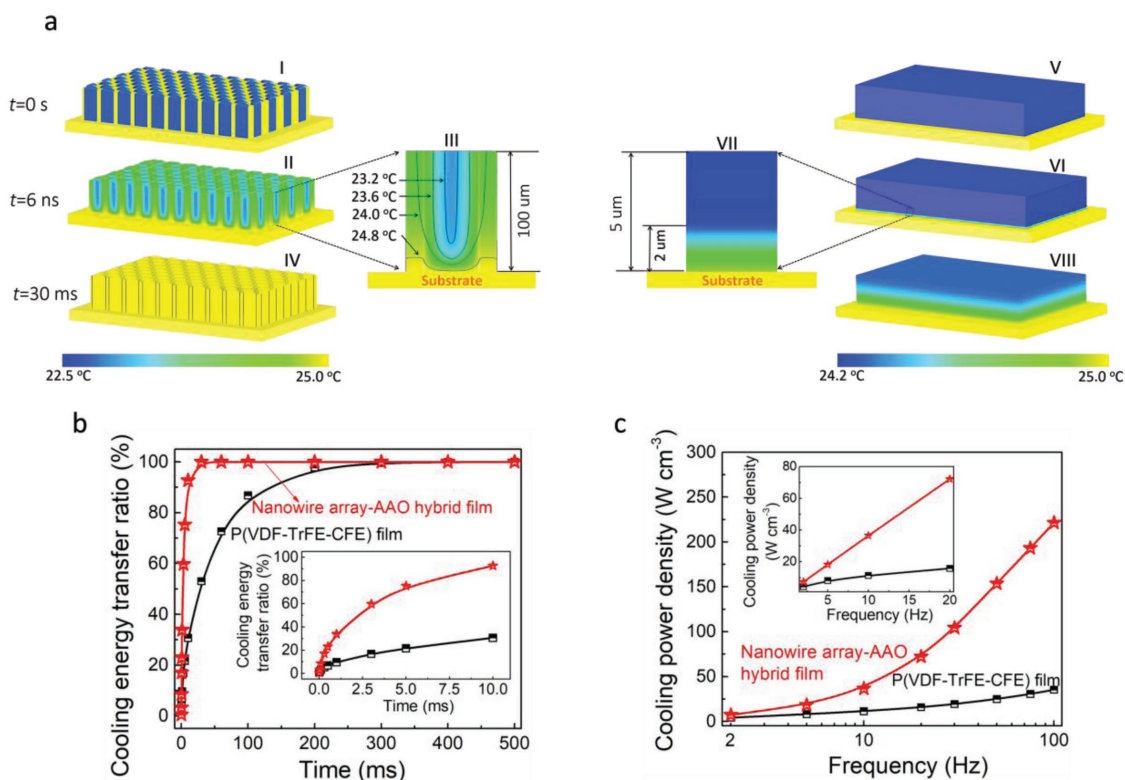


**Figure 4.** a) Simulated heat transfer processes of the integrated hybrid film (left) and the neat polymer film (right) with a thickness of 100  $\mu\text{m}$ . b) The cooling energy transfer ratio of the films as a function of time measured at 50  $\text{MV m}^{-1}$ . Inset: The cooling energy transfer ratio within 10 ms. c) The frequency-dependent cooling energy density of the films at 50  $\text{MV m}^{-1}$ . Inset: The cooling energy density of the films operating from 2 to 20 Hz.

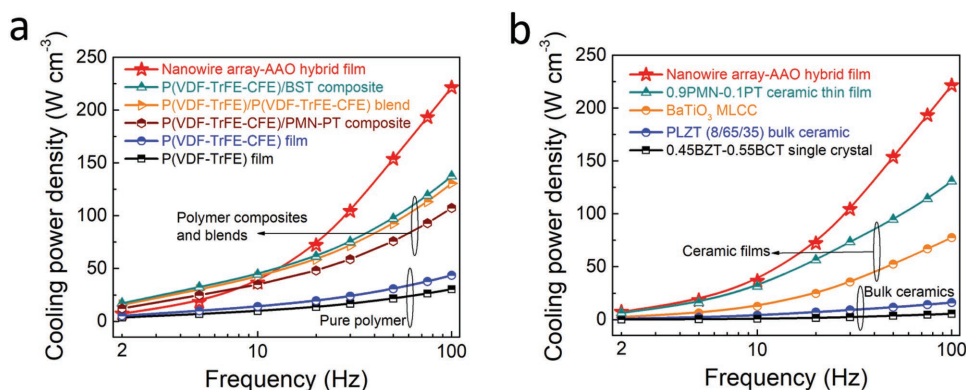
hybrid film flows horizontally along the radii direction and enters the AAO channel walls, as illustrated by the isotherm in Figure 4a-III. Remarkably, a lateral temperature gradient is formed in the nanowire array within an extremely short time interval of 6 ns after the removal of the electric field. In stark contrast, for the pristine polymer film, the temperature gradient along the longitude direction is only observed in the bottom surface next to the substrate within the same period of time (Figure 4a-VI,VII), signifying the limited heat transfer ability of the polymer film. As plotted in Figure 4b, more than 90% of the EC cooling energy of the nanowire array can be absorbed by the substrate within a short time of 10 ms, suggesting a cooling energy transfer ratio  $R_C$  is >90%.  $R_C$  represents the percentage of the energy generated from the EC film that can transfer to the heat load for subsequent cooling. As shown in the inset of Figure 4b, for the conventional polymer film,  $R_C$  is only 30%, i.e., 70% of the cooling energy is retained in the film over the same time interval. The completion of the heat transfer process in the neat polymer film requires  $\approx 400$  ms (Figure 4b).

Figure S17 (Supporting Information) compares  $R_C$  of the neat polymer and the integrated polymer nanowire array-AAO hybrid films as a function of operating frequency. Compared to that of the hybrid film,  $R_C$  of the polymer film decreases much more rapidly with frequency. For example, at 20 Hz, which is the typical frequency of the designed rotary EC device,<sup>[65]</sup>  $R_C$  is 36% of the polymer film versus 98% of the hybrid film. A  $R_C$  that is beyond 80% is maintained in the hybrid film even when the operating frequency is increased to 50 Hz, whereas

$R_C$  is reduced to 22% for the pristine polymer film. The cooling power density ( $D_C$ ) is determined according to  $D_C = Q_E / (\nu \cdot t) = Q_E \cdot f / \nu$ , where  $Q_E = Q \cdot R_C$  is the EC cooling energy that can be effectively absorbed by the load,  $\nu$  is the volume of the EC element,  $t$  is the operating period, and  $f = 1/t$  is the operating frequency.<sup>[30]</sup> Apparently, poor  $R_C$  significantly limits the amount of cooling power per unit volume that can be obtained from the polymer film in spite of its sizable ECE, i.e., large  $Q$ . As shown in Figure 4c,  $D_C$  of the polymer film increases marginally with the operating frequency owing to sharply decreased  $R_C$ . On the other hand, for the integrated hybrid film,  $D_C$  increases nonlinearly with frequency. For instance, at 20 Hz,  $D_C$  of the integrated hybrid film is 72  $W\ \text{cm}^{-3}$ , which is more than three times that of the neat polymer film. When operating at 100 Hz, a record  $D_C$  of 225  $W\ \text{cm}^{-3}$  is achieved in the hybrid film.

More recently, the ECE of the ferroelectric polymers has been improved by more than approximately three times via introducing inorganic fillers such as barium strontium titanate (BST) and lead magnesium niobate-lead titanate (PMN-PT) to form the polymer nanocomposites, and mixing P(VDF-TrFE) and P(VDF-TrFE-CFE) to yield the polymer blends (Table 1).<sup>[21,29,39]</sup> However, their  $D_C$  can only match to those of the integrated hybrid film at frequencies <10 Hz (Figure 5a). Notably, as compared in Figure 5b,  $D_C$  of the hybrid film is much greater than those of the typical inorganic EC materials, especially at high frequencies. For bulk ceramics and single crystals, their  $D_C$  is limited by  $Q$  as a result of low breakdown strength as





**Figure 5.** Comparison of the cooling power density of a) the ferroelectric polymers, polymer nanocomposites, and blends and b) the typical inorganic ferroelectrics to that of the integrated nanowire array-AAO hybrid film.

well as relatively lower thermal conductivity.<sup>[8,22]</sup> The total cooling capacity of the hybrid films can be further improved by stacking the films using a multilayer structure with embedded interdigital electrodes as presented in Figure S18 (Supporting Information).

In summary, we introduced a new design of ferroelectric polymer based EC material composed of the ferroelectric polymer nanowires and the AAO membrane. The increased crystallinity and reduced crystal size under confinement, along with the alignment of the molecular chains and orientation of the crystallites driven by the AAO nanochannels, increase electrical polarization especially at relatively low electric fields. As a result, the polymer nanowires display much improved ECE relative to the corresponding thin films. Concurrently, the integrated AAO membrane facilitates the thermal transfer and has successfully addressed the long-standing challenges of EC materials, thus allowing efficient transfer of EC energy toward the load for cooling and operation of the EC materials at high frequencies. Consequently, the integrated polymer nanowire array-AAO hybrid film exhibits excellent cooling power densities in comparison to the currently available ferroelectric ceramics, polymers, and ceramic-polymer composites. We anticipate that this scalable approach will advance the development of highly efficient and environmentally friendly solid-state cooling technology.

## Supporting Information

Supporting Information is available from the Wiley Online Library or from the author.

## Acknowledgements

The authors acknowledge the support from the National Science Foundation of China (51772108, 61675076, and 61705070), the US National Science Foundation (CMMI1361713), the National Key Research and Development Program of China (2016YFB0402705), and the China Postdoctoral Science Foundation (2017M612449 and 2017T200545). The authors acknowledge the support from the Analytical and Testing Center, Huazhong University of Science and Technology.

## Conflict of Interest

The authors declare no conflict of interest.

## Keywords

cooling power density, electrocaloric effect, ferroelectric polymer, heat transfer, nanoconfinement

Received: October 13, 2018  
Revised: November 13, 2018  
Published online: January 7, 2019

- [1] I. Dincer, *Refrigeration Systems and Applications*, 3rd ed., John Wiley & Sons, West Sussex, UK **2017**, p. 1.
- [2] R. C. Arora, *Refrigeration and Air Conditioning*, PHI Learning Pvt. Ltd., New Delhi **2010**, pp. 1–4.
- [3] J. M. Belman-Flores, J. M. Barroso-Maldonado, A. P. Rodríguez-Muñoz, G. Camacho-Vázquez, *Renewable Sustainable Energy Rev.* **2015**, *51*, 955.
- [4] B. Xiang, P. K. Patra, S. A. Montzka, S. M. Miller, J. W. Elkins, F. L. Moore, E. L. Atlas, B. R. Miller, R. F. Weiss, R. G. Prinn, S. C. Wofsy, *Proc. Natl. Acad. Sci. USA* **2014**, *111*, 17379.
- [5] T. Correia, Q. Zhang, *Electrocaloric Materials: New Generation of Cooler*, Springer-Verlag, Berlin **2014**, pp. 1–3.
- [6] X. Moya, S. Kar-Narayan, N. D. Mathur, *Nat. Mater.* **2014**, *13*, 439.
- [7] X. Moya, D. Emmanuel, V. Heine, N. D. Mathur, *Nat. Phys.* **2015**, *11*, 202.
- [8] V. Franco, J. S. Blázquez, J. J. Ipus, J. Y. Law, L. M. Moreno-Ramírez, A. Conde, *Prog. Mater. Sci.* **2018**, *93*, 112.
- [9] M. Valant, *Prog. Mater. Sci.* **2012**, *57*, 980.
- [10] L. Mañosa, A. Planes, *Adv. Mater.* **2017**, *29*, 1603607.
- [11] Y. Liu, G. Zhang, Q. Li, L. Bellaiche, J. F. Scott, B. Dkhil, Q. Wang, *Phys. Rev. B* **2016**, *94*, 214113.
- [12] A. Aznar, P. Lloveras, M. Romanini, M. Barrio, J.-L. Tamarit, C. Cazorla, D. Errandonea, N. D. Mathur, A. Planes, X. Moya, L. Mañosa, *Nat. Commun.* **2017**, *8*, 1851.
- [13] A. K. Sagotra, D. Errandonea, C. Cazorla, *Nat. Commun.* **2017**, *8*, 963.
- [14] H. Ursic, V. Bobnar, B. Malic, C. Filipic, M. Vrabelj, S. Drnovsek, Y. Jo, M. Wencka, Z. Kutnjak, *Sci. Rep.* **2016**, *6*, 26629.
- [15] R. Ma, Z. Zhang, K. Tong, D. Huber, R. Kornbluh, Y. S. Ju, Q. Pei, *Science* **2017**, *357*, 1130.

- [16] A. S. Mischenko, Q. Zhang, J. F. Scott, R. W. Whatmore, N. D. Mathur, *Science* **2006**, 311, 1270.
- [17] B. Peng, H. Fan, Q. Zhang, *Adv. Funct. Mater.* **2013**, 23, 2987.
- [18] G. Singh, I. Bhaumik, S. Ganesamoorthy, R. Bhatt, A. K. Karnal, V. S. Tiwari, P. K. Gupta, *Appl. Phys. Lett.* **2013**, 102, 082902.
- [19] G. Zhang, X. Zhang, H. Huang, J. Wang, Q. Li, L.-Q. Chen, Q. Wang, *Adv. Mater.* **2016**, 28, 4811.
- [20] B. Neese, B. Chu, S.-G. Lu, Y. Wang, E. Furman, Q. M. Zhang, *Science* **2008**, 321, 821.
- [21] X. Qian, H. J. Ye, T. Yang, W. Z. Shao, L. Zhen, E. Furman, L. Q. Chen, Q. M. Zhang, *Adv. Funct. Mater.* **2015**, 25, 5134.
- [22] J. F. Scott, *Annu. Rev. Mater. Res.* **2011**, 41, 229.
- [23] S. Horiuchi, Y. Tokura, *Nat. Mater.* **2008**, 7, 357.
- [24] S. Kar-Narayan, N. D. Mathur, *Appl. Phys. Lett.* **2009**, 95, 242903.
- [25] Y. Bai, X. Han, X. C. Zheng, L. Qiao, *Sci. Rep.* **2013**, 3, 2895.
- [26] J. E. Mark, *Physical Properties of Polymers Handbook*, Springer, New York **2007**, pp. 156–159.
- [27] S. Crossley, J. R. McGinnigle, S. Kar-Narayan, N. D. Mathur, *Appl. Phys. Lett.* **2014**, 104, 082909.
- [28] H. M. Gu, X. S. Qian, X. Y. Li, B. Craven, W. Y. Zhu, A. Cheng, S. C. Yao, Q. M. Zhang, *Appl. Phys. Lett.* **2013**, 102, 112901.
- [29] G. Zhang, B. Fan, P. Zhao, Z. Hu, Y. Liu, F. Liu, S. Jiang, S. Zhang, H. Li, Q. Wang, *ACS Appl. Energy Mater.* **2018**, 1, 1344.
- [30] G. Zhang, Q. Li, H. Gu, S. Jiang, K. Han, M. R. Gadinski, M. A. Haque, Q. Zhang, Q. Wang, *Adv. Mater.* **2015**, 27, 1450.
- [31] G. Zhang, X. Zhang, T. Yang, Q. Li, L.-Q. Chen, S. Jiang, Q. Wang, *ACS Nano* **2015**, 9, 7164.
- [32] W. Lee, S.-J. Park, *Chem. Rev.* **2014**, 114, 7487.
- [33] A. S. Mischenko, Q. Zhang, R. W. Whatmore, J. F. Scott, N. D. Mathur, *Appl. Phys. Lett.* **2006**, 89, 242912.
- [34] J. Chen, Z. Tang, Q. Lu, S. Zhao, *J. Alloys Compd.* **2018**, 756, 62.
- [35] F. Guo, X. Wu, Q. Lu, S. Zhao, *Ceram. Int.* **2018**, 44, 2803.
- [36] S. Kar-Narayan, N. D. Mathur, *J. Phys. D: Appl. Phys.* **2010**, 43, 032002.
- [37] R. Selvamani, G. Singh, V. S. Tiwari, *AIP Conf. Proc.* **2012**, 1447, 1281.
- [38] X. Li, X.-S. Qian, H. Gu, X. Chen, S. G. Lu, M. Lin, F. Bateman, Q. M. Zhang, *Appl. Phys. Lett.* **2012**, 101, 132903.
- [39] Q. Li, G. Zhang, X. Zhang, S. Jiang, Y. Zeng, Q. Wang, *Adv. Mater.* **2015**, 27, 2236.
- [40] A. Houachtia, P. Alcouffe, G. Boiteux, G. Seytre, J. F. Gérard, A. Serghei, *Nano Lett.* **2015**, 15, 4311.
- [41] B. D. Cullity, *Elements of X-ray Diffraction*, Addison Wesley, MA, USA **1978**, pp. 102.
- [42] P. B. Rim, J. P. Runt, *Macromolecules* **1984**, 17, 1520.
- [43] Y. Kong, J. N. Hay, *Polymer* **2002**, 43, 3873.
- [44] J. Li, J. Claude, L. E. Norena-Franco, S. Il Seok, Q. Wang, *Chem. Mater.* **2008**, 20, 6304.
- [45] Q. Li, G. Zhang, F. Liu, K. Han, M. R. Gadinski, C. Xiong, Q. Wang, *Energy Environ. Sci.* **2015**, 8, 922.
- [46] S. G. Lu, B. Rozic, Q. M. Zhang, Z. Kutnjak, R. Pirc, *Appl. Phys. A* **2012**, 107, 559.
- [47] H. Pan, J. Ma, J. Ma, Q. Zhang, X. Liu, B. Guan, L. Gu, X. Zhang, Y.-J. Zhang, L. Li, Y. Shen, Y.-H. Lin, C.-W. Nan, *Nat. Commun.* **2018**, 9, 1813.
- [48] L. Wu, X. Wang, Z. Shen, L. Li, *J. Am. Ceram. Soc.* **2017**, 100, 265.
- [49] H. Ogihara, C. A. Randall, S. Trolrier-McKinstry, *J. Am. Ceram. Soc.* **2009**, 92, 110.
- [50] Y. Ma, W. Hu, J. Hobbs, G. Reiter, *Soft Matter* **2008**, 4, 540.
- [51] M. Wang, W. Hu, Y. Ma, Y. Q. Ma, *J. Chem. Phys.* **2006**, 124, 244901.
- [52] X. Li, Y. F. Lim, K. Yao, F. E. H. Tay, K. H. Seah, *Chem. Mater.* **2013**, 25, 524.
- [53] Z. Hu, G. Baralia, V. Bayot, J. F. Gohy, A. M. Jonas, *Nano Lett.* **2005**, 5, 1738.
- [54] M. C. García-Gutiérrez, A. Linares, J. J. Hernández, D. R. Rueda, T. A. Ezquerro, P. Poza, R. J. Davies, *Nano Lett.* **2010**, 10, 1472.
- [55] V. Cauda, S. Stassi, K. Bejtka, G. Canavese, *ACS Appl. Mater. Interfaces* **2013**, 5, 6430.
- [56] Z. Hu, M. Tian, B. Nysten, A. M. Jonas, *Nat. Mater.* **2009**, 8, 62.
- [57] V. Bhavanasri, D. Y. Kusuma, P. S. Lee, *Adv. Energy Mater.* **2014**, 4, 1400723.
- [58] M. Ožbolt, A. Kitanovski, J. Tušek, A. Poredoš, *Int. J. Refrig.* **2014**, 40, 174.
- [59] C. Aprea, A. Greco, A. Maiorino, *Int. J. Energy Res.* **2011**, 35, 177.
- [60] C. A. Randall, N. Kim, J.-P. Kucera, W. Cao, T. R. Shrout, *J. Am. Ceram. Soc.* **1998**, 81, 677.
- [61] S. Roy, P. Sarah, *J. Phys. D: Appl. Phys.* **2007**, 40, 4668.
- [62] L. Yang, X. Li, E. Allahyarov, P. L. Taylor, Q. M. Zhang, L. Zhu, *Polymer* **2013**, 54, 1709.
- [63] Y. He, *Thermochim. Acta* **2004**, 419, 135.
- [64] B. M. Foley, E. A. Paisley, C. DiAntonio, T. Chavez, M. Blea-Kirby, G. Brennecke, J. T. Gaskins, J. F. Ihlefeld, P. E. Hopkins, *J. Appl. Phys.* **2017**, 121, 205104.
- [65] H. Gu, X. Qian, H.-J. Ye, Q. M. Zhang, *Appl. Phys. Lett.* **2014**, 105, 162905.